PUBLICATION V

Incorporating sensitivity and uncertainty analysis to a lattice physics code with application to CASMO-4

In: Annals of Nuclear Energy,
40, 1, pp. 153–162.

Annals of Nuclear Energy 40 (2012) 153–162

Contents lists available at SciVerse ScienceDirect

Annals of Nuclear Energy

journal homepage: www.elsevier.com/locate/anucene

Incorporating sensitivity and uncertainty analysis to a lattice physics code with application to CASMO-4

Maria Pusa *

VTT Technical Research Centre of Finland, Nuclear Energy, P.O. Box 1000, FI-02044 VTT, Finland

ARTICLE INFO

Article history:
Received 20 May 2011
Received in revised form 17 October 2011
Accepted 18 October 2011
Available online 1 December 2011

Keywords:
Sensitivity analysis
Uncertainty analysis
Perturbation theory

ABSTRACT

This paper describes the implementation of classical perturbation theory based sensitivity and uncertainty analysis to the reactor physics code CASMO-4 in the context of the UAM (Uncertainty Analysis in Best-Estimate Modelling for Design, Operation and Safety Analysis of LWRS) benchmark. The theoretical background as well as practical guidelines for similar work are reviewed and the developed methodology is described in detail. A technique is proposed for handling a discrepancy between the code and covariance libraries regarding the amount of reactions present in the cross-section model. Numerical results for PWR and GEN-III MOX pin-cell test problems are presented and compared to TSUNAMI-1D. The results are in accordance with theoretical considerations and reflect the characteristics of the developed methodology.

1. Introduction

In recent years the interest towards sensitivity and uncertainty (S&U) analysis has increased notably in the field of nuclear engineering. In 2006, the OECD/NEA expert group on Uncertainty Analysis in Modelling decided to prepare a benchmark titled *Uncertainty Analysis in Best-Estimate Modelling (UAM) for Design, Operation and Safety Analysis of LWRs* (Ivanov et al., 2011) to establish the current state and needs of S&U analysis. The goal of the benchmark is to propagate uncertainty through all stages of coupled neutronics/thermal hydraulics calculations. The imprecision of neutron cross-sections is likely one of the most significant sources of uncertainty in these calculations, and therefore the propagation of this uncertainty is the main priority in the benchmark at the moment. As a first step, this requires developing S&U analysis methods for reactor physics codes that are used to produce homogenized data for coupled neutronics/thermal-hydraulics calculations.

The objective of the benchmark is fairly ambitious as the commonly used reactor physics codes, such as CASMO (Rhodes and Edenius, 2001), HELIOS (HELIOS, 2000), and NEWT (DeHart, 2009), do not have S&U analysis capabilities. In addition, incorporating S&U features to such codes can be quite involved, if the code was not designed from this perspective in the first place. In particular, if a lattice physics code is based on a cross-section model, where the individual capture and scattering reactions have been combined to total scattering and capture reactions, respectively, this will cause complications because the covariance matrices are always reported for the individual reactions. This applies to both statistical and deterministic uncertainty analysis. For example, the lattice physics codes CASMO, HELIOS, WIMS (WIMS9A, 2005), and DRAGON (Marleau et al., 2009) all have a similar cross-section model that is based on combining the individual capture and scattering cross-sections.

At VTT, the UAM benchmark was recognized as an opportunity to start developing an S&U analysis calculation system. Since CASMO-4 is the standard tool for lattice physics calculations at VTT, it was decided to begin developing S&U analysis capability to it. As a first step, classical perturbation theory (CPT) has been implemented to enable the computation of critical eigenvalue sensitivities with respect to cross-sections. In addition, a methodology was developed for processing the covariance matrices from SCALE 6 (NEA Data Bank, 2011) to become compatible with the cross-section model of CASMO-4 to enable uncertainty analysis. This processing methodology has since been adopted by other participants in the UAM benchmark (Wieselquist et al., 2011). In addition to describing the developed methodology, the purpose of this paper is to review the theoretical background and practical guidelines for implementing S&U methods to lattice physics codes. Emphasis is put on dealing with the cross-section model of CASMO-4.

2. Theoretical background

The purpose of sensitivity analysis is to study how sensitive a mathematical model is to perturbations in its uncertain parameters. The objective of uncertainty analysis is to estimate how the uncertainty in these parameters is propagated to a response

* Tel.: +358 40 756 8257; fax: +358 20 722 5000.
E-mail address: Maria.Pusa@vtt.fi

0306-4549/$ - see front matter © 2011 Elsevier Ltd. All rights reserved.
doi:10.1016/j.anucene.2011.10.013

dependent on the mathematical model under consideration. In this work the mathematical model is the neutron transport criticality equation, which is an eigenvalue problem that can be written in operator form as

$$\boldsymbol{A}\boldsymbol{\Phi} = \frac{1}{k}\boldsymbol{B}\boldsymbol{\Phi}, \tag{1}$$

where $\boldsymbol{\Phi} \in H_\Phi$ is the neutron flux, H_Φ is a Hilbert space and k is the multiplication factor. It should be noted that both the continuous-energy criticality equation and the various systems derived from it in numerical computations can be written in the form of Eq. (1). The uncertain parameters are the neutron cross-sections and they are denoted by $\boldsymbol{\sigma} \in E_\sigma$, where E_σ is a normed space. The response R under consideration is the critical eigenvalue k, which forms a special case in terms of sensitivity analysis and can be treated with classical perturbation theory as described in the following section.

2.1. Sensitivity analysis

The object of local sensitivity analysis is to determine how the multiplication factor k depends on the cross-sections near their evaluated value $\hat{\boldsymbol{\sigma}}$. This dependence is characterized by the directional derivative of the response in the direction of the perturbation $\delta\boldsymbol{\sigma}$. When considering the continuous-energy criticality equation, the cross-sections are functions of energy and location, and the appropriate derivative is the functional directional derivative called the Gâteaux-variation (Cacuci, 2003). It follows that the sensitivity of R with respect to the perturbation $\boldsymbol{h} = [\delta\boldsymbol{\Phi}, \delta\boldsymbol{\sigma}] \in D = H_\Phi \times E_\sigma$ at the point $\hat{\boldsymbol{e}} = [\boldsymbol{\Phi}, \hat{\boldsymbol{\sigma}}] \in D$ may be defined as:

$$\delta R(\hat{\boldsymbol{e}}; \boldsymbol{h}) = \lim_{t\to 0} \frac{R(\hat{\boldsymbol{e}} + t\boldsymbol{h}) - R(\hat{\boldsymbol{e}})}{t}. \tag{2}$$

When the cross-sections are perturbed, also the solution $\boldsymbol{\Phi}$ is affected and therefore the computation of the sensitivity $\delta R(\hat{\boldsymbol{e}}; \boldsymbol{h})$ requires that the perturbation $\delta\boldsymbol{\Phi}$ is known. In principle, $\delta\boldsymbol{\Phi}$ can be computed from the following *forward sensitivity system*:

$$\delta k(\hat{\boldsymbol{e}}; \boldsymbol{h})\boldsymbol{A}\boldsymbol{\Phi} + k\delta\boldsymbol{A}(\hat{\boldsymbol{e}}; \boldsymbol{h}) = \delta\boldsymbol{B}(\hat{\boldsymbol{e}}; \boldsymbol{h}), \tag{3}$$

which can be derived by taking the Gâteaux-variation of system (1) with respect to a perturbation $\boldsymbol{h}$ on both sides. However, when computing several sensitivities, this approach would require the repetitive solving of Eq. (3).

Fortunately, the sensitivities can be computed more efficiently by exploiting the adjoint of Eq. (1), which is defined as the system that satisfies the following relation[1]:

$$\left\langle \boldsymbol{A}\boldsymbol{\Phi} - \frac{1}{k}\boldsymbol{B}\boldsymbol{\Phi}, \boldsymbol{\Psi} \right\rangle = \left\langle \boldsymbol{\Phi}, \boldsymbol{A}^*\boldsymbol{\Psi} - \frac{1}{k}\boldsymbol{B}^*\boldsymbol{\Psi} \right\rangle \tag{4}$$

where the brackets $\langle \cdot, \cdot \rangle$ denote an inner product. When considering the continuous-energy criticality equation, it is customary to employ the L^2 inner product (Carlson and Lathrop, 1968; Lewis and Miller, 1984). The expression for the sensitivity (3) can now be written utilizing this adjoint relation. Since the operators $\boldsymbol{A}$ and $\boldsymbol{B}$ are linear with respect to $\boldsymbol{\Phi}$, they are also Fréchet-differentiable with respect to $\boldsymbol{\Phi}$ with $\boldsymbol{A}'_\Phi = \boldsymbol{A}$ and $\boldsymbol{B}'_\Phi = \boldsymbol{B}$. Eq. (3) can thus be written in the form:

$$\delta k(\hat{\boldsymbol{e}}; \boldsymbol{h})\boldsymbol{A}\boldsymbol{\Phi} + k\boldsymbol{A}'_\sigma(\hat{\boldsymbol{e}})\ \delta\boldsymbol{\sigma} + k\boldsymbol{A}(\hat{\boldsymbol{e}})\ \delta\boldsymbol{\Phi} = \boldsymbol{B}'_\sigma(\hat{\boldsymbol{e}})\ \delta\boldsymbol{\sigma} + \boldsymbol{B}(\hat{\boldsymbol{e}})\ \delta\boldsymbol{\Phi}. \tag{5}$$

For any $\boldsymbol{\Psi} \in H_\Phi$ not orthogonal with $\boldsymbol{A}\boldsymbol{\Phi}$ or $\boldsymbol{B}\boldsymbol{\Phi}$, it now holds:

$$\begin{aligned}
\delta k(\hat{\boldsymbol{e}}; \boldsymbol{h}) &= \frac{\left\langle (-k\boldsymbol{A}'_\sigma + \boldsymbol{B}'_\sigma)\delta\boldsymbol{\sigma}, \boldsymbol{\Psi} \right\rangle + \left\langle (-k\boldsymbol{A} + \boldsymbol{B})\delta\boldsymbol{\Phi}, \boldsymbol{\Psi} \right\rangle}{\langle \boldsymbol{A}\boldsymbol{\Phi}, \boldsymbol{\Psi} \rangle} \\
&= -\frac{\left\langle (\boldsymbol{A}'_\sigma - \frac{1}{k}\boldsymbol{B}'_\sigma)\delta\boldsymbol{\sigma}, \boldsymbol{\Psi} \right\rangle + \left\langle (\boldsymbol{A} - \frac{1}{k}\boldsymbol{B})\delta\boldsymbol{\Phi}, \boldsymbol{\Psi} \right\rangle}{\left\langle \frac{1}{k^2}\boldsymbol{B}\boldsymbol{\Phi}, \boldsymbol{\Psi} \right\rangle} \\
&= -\frac{\left\langle (\boldsymbol{A}'_\sigma - \frac{1}{k}\boldsymbol{B}'_\sigma)\delta\boldsymbol{\sigma}, \boldsymbol{\Psi} \right\rangle + \left\langle \delta\boldsymbol{\Phi}, (\boldsymbol{A}^* - \frac{1}{k}\boldsymbol{B}^*)\boldsymbol{\Psi} \right\rangle}{\left\langle \frac{1}{k^2}\boldsymbol{B}\boldsymbol{\Phi}, \boldsymbol{\Psi} \right\rangle}.
\end{aligned} \tag{6}$$

If the function $\boldsymbol{\Psi}$ is chosen as the solution of the adjoint system

$$\left(\boldsymbol{A}^* - \frac{1}{k}\boldsymbol{B}^*\right)\boldsymbol{\Psi} = 0 \tag{7}$$

the response sensitivity may be computed as

$$\delta k(\hat{\boldsymbol{e}}; \boldsymbol{h}) = -\frac{\left\langle (\boldsymbol{A}'_\sigma - \frac{1}{k}\boldsymbol{B}'_\sigma)\delta\boldsymbol{\sigma}, \boldsymbol{\Psi} \right\rangle}{\left\langle \frac{1}{k^2}\boldsymbol{B}\boldsymbol{\Phi}, \boldsymbol{\Psi} \right\rangle} \tag{8}$$

which is known as classical perturbation theory in reactor physics.

In practice the criticality equation and the corresponding adjoint equation are solved numerically, which gives rise to some complications in the CPT formalism. Ideally, the numerical method applied to computing the sensitivities should fulfill two conditions. Firstly, the discretized forward and adjoint systems and the discretized operators corresponding to the functional derivatives A'_σ and B'_σ should be consistent with the analytical equations (Cacuci, 2003). Secondly, the inner product in (8) should be discretized in a manner consistent with the discretized operators thereby bringing the operators into a Hilbert-space, where the discretized operators are adjoints with respect to the discretized inner product (Cacuci, 2003).

However, this type of consistent sensitivity analysis is usually infeasible in reactor physics calculations. For example, if the multi-group approximation is applied to the continuous-energy forward and adjoint systems, this leads to two sets of multi-group cross-sections—one weighted with the energy spectrum corresponding to the forward system and one weighted with the energy spectrum corresponding to the adjoint system. For this reason, it is customary to take the multi-group criticality equation as the starting point and apply CPT to it. Another common approach is to apply the discrete ordinates approximation before formulating the CPT setup. As previously noted, after these approximations the criticality equation can still be written as a system of the form of Eq. (1), where $\boldsymbol{\Phi}$ is now a vector. The inner product corresponding to this system can be defined in a consistent manner as

$$\langle \boldsymbol{\Phi}, \boldsymbol{\Psi} \rangle = \sum_{g=1}^{G} \sum_{m=1}^{M} \omega_m \int_D d^3\boldsymbol{r}\, \Phi^g(\boldsymbol{r}, \boldsymbol{\Omega}_m)\Psi^g(\boldsymbol{r}, \boldsymbol{\Omega}_m) \tag{9}$$

where $\{\boldsymbol{\Omega}_m\}$ are the considered directions in the discrete ordinates approximation and ω_m are the associated quadrature weights. After fixing the boundary conditions for the forward problem, the adjoint system and its boundary conditions can be determined based on Eq. (4).

2.2. Uncertainty analysis

The uncertainty of the cross-sections $\boldsymbol{\sigma}$ should be understood in terms of the Bayesian probability interpretation. In this framework, all knowledge about a parameter σ is presented as a probability distribution and the spread of this distribution characterizes the uncertainty related to σ. Typically, the variance of the distribution is chosen to give a numerical value to this uncertainty. When several parameters are considered simultaneously, the probability distribution under consideration is their joint distribution $p(\boldsymbol{\sigma})$, and the covariance matrix of this distribution may be chosen as the

[1] In some cases it is more convenient to write the adjoint relation in the form $\langle \boldsymbol{A}\boldsymbol{\Phi} + \frac{1}{k}\boldsymbol{B}\boldsymbol{\Phi}, \boldsymbol{\Psi} \rangle = \langle \Phi, \boldsymbol{A}^*\boldsymbol{\Psi} + \frac{1}{k}\boldsymbol{B}^*\boldsymbol{\Psi} \rangle + [\boldsymbol{P}(\boldsymbol{\Psi}, \boldsymbol{\Phi})]_{\boldsymbol{x}\in\partial\Omega}$ where $[\boldsymbol{P}(\boldsymbol{\Psi}, \boldsymbol{\Phi})]_{\boldsymbol{x}\in\partial\Omega}$ is a bilinear form associated with the system. We will only consider cases where it is straightforward to force this term to vanish.

descriptive statistic for the uncertainty. The uncertainty related to cross-sections is generally reported as covariance matrices.

In the Bayesian formalism, the outcome of the uncertainty analysis should ideally be the posterior distribution $p(R)$ containing all knowledge about the response R under consideration. However, determining $p(R)$ is usually extremely challenging and can often only be done based on a simulation. Therefore, a common practice is to compute estimates for the mean and variance of $p(R)$ and assume the distribution to be Gaussian. Typically the estimate for $\mathrm{Var}[R]$ is obtained by linearizing $R \approx \boldsymbol{s}\boldsymbol{\sigma}$, where $\boldsymbol{s} \in \mathbb{R}^{1\times K}$, and using the identity

$$\mathrm{Var}[R] \approx \mathrm{Var}[\boldsymbol{s}\boldsymbol{\sigma}] = \boldsymbol{s}\mathrm{Cov}[\boldsymbol{\sigma}]\boldsymbol{s}^T \tag{10}$$

known as the *Sandwich rule*. Eq. (10) can be generalized to several responses $\boldsymbol{R} \in \mathbb{R}^J$ as:

$$\mathrm{Cov}[\boldsymbol{R}] = \boldsymbol{S}\mathrm{Cov}[\boldsymbol{\sigma}]\boldsymbol{S}^T \tag{11}$$

where $\boldsymbol{S} \in \mathbb{R}^{J\times K}$. This procedure is exact when $\boldsymbol{R}$ depends linearly on the parameters and $p(\boldsymbol{\sigma})$ is a Gaussian distribution. If $\boldsymbol{\sigma}$ obeys a Gaussian distribution with mean $\hat{\boldsymbol{\sigma}}$ and covariance matrix $\mathrm{Cov}[\boldsymbol{\sigma}]$, i.e. $\boldsymbol{\sigma} \sim \mathrm{N}(\hat{\boldsymbol{\sigma}}, \mathrm{Cov}[\boldsymbol{\sigma}])$, it follows that

$$\boldsymbol{\eta} = \boldsymbol{c} + \boldsymbol{S}\boldsymbol{\sigma} \sim \mathrm{N}(\boldsymbol{c} + \boldsymbol{S}\hat{\boldsymbol{\sigma}}, \boldsymbol{S}\mathrm{Cov}[\boldsymbol{\sigma}]\boldsymbol{S}^T) \tag{12}$$

where $\boldsymbol{c} \in \mathbb{R}^K$ is a constant vector and $\boldsymbol{S}$ is a constant matrix. Therefore, in this special case, the Sandwich rule yields the exact posterior distribution for the response $\boldsymbol{\eta}$.

3. Implementation

3.1. Computation of adjoint flux

It is generally quite straightforward to modify a deterministic transport solver to also run in adjoint mode. This section reviews the guidelines for this procedure and describes the methodology used in implementing an adjoint solver to CASMO-4.

In CASMO-4, the multi-group criticality equation is solved by the method of characteristics assuming isotropic scattering. Therefore, the following system of equations may be taken as the forward problem:

$$\begin{aligned}&\boldsymbol{\Omega}_m \cdot \nabla \Phi^g(\boldsymbol{r}, \boldsymbol{\Omega}_m) + \Sigma^g \Phi^g(\boldsymbol{r}, \boldsymbol{\Omega}_m)\\ &\quad = \frac{1}{4\pi}\sum_{h=1}^{G} \Sigma_s^{h\to g}\phi^h(\boldsymbol{r}) + \frac{\chi_g}{4\pi k}\sum_{h=1}^{G} \bar{\nu}\Sigma_f^h \phi^h(\boldsymbol{r}), \quad g = 1,\ldots,G.\end{aligned} \tag{13}$$

In Eq. (13) the scalar flux is approximated by the quadrature formula

$$\phi^h(\boldsymbol{r}) = \sum_{m=1}^{M} \omega_m \Phi^h(\boldsymbol{r}, \boldsymbol{\Omega}_m). \tag{14}$$

In order to simulate an infinite lattice, the boundary conditions are often assumed to be reflective, i.e.

$$\boldsymbol{\Phi}(\boldsymbol{r}, \boldsymbol{\Omega}_m, E) = \boldsymbol{\Phi}(\boldsymbol{r}, \boldsymbol{\Omega}'_m, E) \quad \boldsymbol{r} \in \Gamma,\ \boldsymbol{\Omega}_m \cdot \boldsymbol{n} < 0 \tag{15}$$

where $\boldsymbol{\Omega}_m = \boldsymbol{\Omega}'_m - 2(\boldsymbol{n}\cdot\boldsymbol{\Omega}'_m)\,\boldsymbol{n}$ is the reflection direction. The adjoint system corresponding to the inner product defined by Eq. (9) can now be written

$$\begin{aligned}&-\boldsymbol{\Omega}_m \cdot \nabla \Psi^g(\boldsymbol{r}, \boldsymbol{\Omega}_m) + \Sigma^g \Psi^g(\boldsymbol{r}, \boldsymbol{\Omega}_m)\\ &\quad = \frac{1}{4\pi}\sum_{h=1}^{G} \Sigma_s^{g\to h}\psi^h(\boldsymbol{r}) + \frac{\bar{\nu}\Sigma_f^g}{4\pi k}\sum_{h=1}^{G} \chi_h \psi^h(\boldsymbol{r}), \quad g = 1,\ldots,G\end{aligned} \tag{16}$$

with the boundary conditions

$$\boldsymbol{\Psi}(\boldsymbol{r}, \boldsymbol{\Omega}_m, E) = \boldsymbol{\Psi}(\boldsymbol{r}, \boldsymbol{\Omega}'_m, E) \quad \boldsymbol{r} \in \Gamma,\ \boldsymbol{\Omega}_m \cdot \boldsymbol{n} > 0. \tag{17}$$

It is straightforward to check that systems (13) and (16) with their respective boundary conditions satisfy Eq. (4) with respect to the inner product defined by Eq. (9).

When solving the system of Eq. (13) numerically, the eigenvalue and flux are iterated in turns. The iteration step for the flux can typically be written

$$\boldsymbol{A}\boldsymbol{\Phi}^{n+1} = \frac{1}{k^n}\boldsymbol{B}\boldsymbol{\Phi}^n. \tag{18}$$

After solving $\boldsymbol{\Phi}^{n+1}$ from this equation, a new estimate is obtained for the multiplication factor according to

$$k^{n+1} = \frac{\langle \boldsymbol{w}, \boldsymbol{B}\boldsymbol{\Phi}^{n+1}\rangle}{\langle \boldsymbol{w}, \boldsymbol{A}\boldsymbol{\Phi}^{n+1}\rangle} = k^n \frac{\langle \boldsymbol{w}, \boldsymbol{B}\boldsymbol{\Phi}^{n+1}\rangle}{\langle \boldsymbol{w}, \boldsymbol{B}\boldsymbol{\Phi}^{n}\rangle} \tag{19}$$

where $\boldsymbol{w}$ is a weighting function. This approach is also well-suited for solving the adjoint system. In CASMO-4, however, the eigenvalue iteration is based on physical considerations, and therefore it was replaced by the conventional power iteration based on Eq. (19) before adding the adjoint mode to the code.

Solving Eq. (18) forms an essential part of the iteration. By comparing the forward system (13) to the adjoint system (16), it can be seen that the systems are of the same form, but the adjoint system has a different source and it is solved in the opposite direction. This property may be exploited by using the inner iterations solver with a modified input for the adjoint system (Williams, 1986). This can be achieved by performing the following operations before the adjoint calculation:

1. Transpose the scattering matrix
2. Interchange the vectors $\bar{\nu}\boldsymbol{\sigma}_f$ and $\boldsymbol{\chi}$
3. Invert the group indices as follows: $G \leftrightarrow 1$, $(G-1) \leftrightarrow 2, \ldots$

The solution given by the forward solver must then be interpreted so that $\Phi_i^g(\boldsymbol{r}_k, \boldsymbol{\Omega}_m)$ corresponds to $\Psi_i^{G+1-g}(\boldsymbol{r}_k, -\boldsymbol{\Omega}_m)$. Notice that these operations automatically convert the forward boundary conditions to the adjoint boundary conditions. Therefore, only minor modifications are often needed to solve the adjoint flux with a transport code.

The so far described methodology does not ensure that the consistency objectives discussed in Section 2.1 are met. As previously mentioned, the numerical method used in the inner iterations should ideally produce discretized systems that are adjoints with respect to the discretized inner product. When an iteration based on Eqs. (18) and (19) is used, it is guaranteed that both systems converge to the same eigenvalue. Unfortunately, many of the established numerical methods do not enable this type of consistency. For example, the very popular diamond difference method does not guarantee adjointness in curved geometries (Greenspan, 1982). The method of characteristics used in CASMO-4, on the other hand, is not well-suited for this type of formal analysis, since it does not directly provide a discretization scheme that could be used to check if Eq. (4) holds. For these reasons, the inner product of Eq. (9) was approximated as

$$\langle \boldsymbol{\Phi}, \boldsymbol{\Psi}\rangle \approx \sum_{i=1}^{I}\sum_{g=1}^{G}\sum_{m=1}^{M} \omega_m\, V_i\, \overline{\Phi}^{g,i,m}\overline{\Psi}^{g,i,m} \tag{20}$$

where i denotes the mesh index and $\overline{\Phi}^{g,i,m}$ and $\overline{\Psi}^{g,i,m}$ denote the average fluxes. Notice that this discretization can be used with any type of numerical method including multi-group Monte Carlo techniques (Rearden, 2009).

3.2. Computation of sensitivity and uncertainty profiles

After obtaining the adjoint solution, the sensitivities with respect to the multi-group cross-sections and other parameters

of interest can be computed according to Eq. (8). Notice that even after the multi-group approximation, these parameters are still spatial functions and therefore the derivatives in Eq. (8) refer to functional derivatives. After obtaining expressions for all derivatives $\boldsymbol{A}'_\sigma$ and $\boldsymbol{B}'_\sigma$ of interest, the respective sensitivities may be computed simply by applying the discretization scheme of Eq. (9) to Eq. (8).

In order to compute the uncertainties using the Sandwich rule, the sensitivities and covariance matrices need to be based on similar cross-section models. However, as mentioned in Section 1, lattice physics codes such as CASMO, HELIOS, WIMS and DRAGON, have cross-section models different from the one used in the covariance files. More specifically, their cross-section models only contain the total capture and scattering cross-sections, whereas the covariance data is reported for the individual capture and scattering subreactions. This greatly complicates the implementation of uncertainty analysis with both deterministic and statistical methods, since the prerequisite for uncertainty analysis is that the probability distributions for the parameters used in the calculation are known.

Naturally, this difficulty can be overcome by creating new nuclear data libraries and modifying the cross-section model in the code, but this requires extensive work. Another option, suitable for deterministic analysis, is to not use problem-dependent cross-sections in the sensitivity analysis. In this case, the sensitivity coefficients can be computed outside the code based on the forward and adjoint fluxes and any set of cross-sections. This was the idea, for example, behind connecting DRAGON with the sensitivity and uncertainty analysis code SUSD3D After a generalized adjoint mode was implemented to DRAGON (Bidaud et al., 2009).

In this work, this complication was solved by the novel approach of creating a covariance library that is consistent with the cross-section model of CASMO-4. In practice this requires combining the covariance matrices of the individual capture and scattering reactions. Interestingly, this treatment of covariance matrices draws attention to the significance of some basic assumptions made in sensitivity analysis. This approach is explained next by first describing the procedure used to process the covariance matrices to the energy-group structure of CASMO-4, and then considering the methodology for combining the capture and scattering reactions.

3.2.1. Modifying the energy-group structure of covariance matrices

Applying the Sandwich rule requires a covariance library in the same energy-group structure as the sensitivity profiles used in the uncertainty computation. When the starting point is a multi-group covariance library, the matrices can in principle be transformed to another multi-group structure by simple mathematical techniques. The applicability of this approach depends on the differences between the group-structures. In particular, the widths of the energy groups should not be drastically different. In this work, the covariance data was taken from the multi-group covariance library ZZ-SCALE6.0/COVA-44G (NEA Data Bank, 2011) and the code Angelo 2.3 (Kodeli, 2010) was used for transforming the matrices to the energy-group structure used in the sensitivity calculations with CASMO-4.

The transformation procedure in Angelo 2.3 is based on a flat-flux approximation, i.e. no weighting is used in the process. Covariance matrices are treated as correlation matrices and relative standard deviations, whose values are computed separately on the new energy grid. The resampled values on the new grid are computed as lethargy overlap weighted averages. This guarantees that the integrals over the new energy groups remain constant in the resampling process. When the new energy groups extend outside the region spanned by the original energy groups, a complete correlation is assumed with the group from which the extrapolation is carried out (Kodeli and Sartori, 1990).

Because the fission spectrum always satisfies the normalization condition

$$\sum_{g=1}^{G} \chi_g = 1 \tag{21}$$

it follows that the corresponding covariance matrix $\boldsymbol{C}_\chi$ should satisfy the constraint that the sum of the elements on any row of the matrix equals zero, which is also stated in the manual for the ENDF-6 format (Herman and Trkov, 2009). When the energy group structure of $\boldsymbol{C}_\chi$ is modified, there is no guarantee that this constraint is satisfied, which may in turn lead to an erroneously large fission spectrum uncertainty in a criticality calculation (Kodeli et al., 2008). If this zero-sum rule is not too severely violated, there is a suggested correction procedure for the matrix in the ENDF-6 manual.

However, it is often more practical to apply the correction directly to the sensitivity coefficients. In this case the coefficients are called *constrained*. The absolute constrained sensitivities are defined as

$$\boldsymbol{s}_{\text{constr.}} = (\boldsymbol{I} - \boldsymbol{u}\boldsymbol{\chi}^T)\boldsymbol{s}_\chi \tag{22}$$

where $\boldsymbol{I} \in \mathbb{R}^{G\times G}$ is an identity matrix, $\boldsymbol{u} = [1, 1, \ldots, 1]^T$ and vector $\boldsymbol{s}_\chi$ contains the unconstrained sensitivities. In case of a small deviation from the zero-sum rule, applying this correction to the sensitivities is identical to the correction scheme suggested in the ENDF-6 manual. It is easy to see that if the matrix $\boldsymbol{C}_\chi$ already satisfies the zero-sum rule, constraining the sensitivities has no effect on the results (Kodeli et al., 2008). This approach was also applied in this work.

3.2.2. S&U analysis of capture cross-section

Generally, the total capture cross-section is defined as the sum of the individual capture cross-sections (ENDF/MT 102–107). In CASMO-4, however, also the (n,2n) cross-section (ENDF/MT 16) has been added to the capture cross-section with a negative sign in the highest energy group. The expression for a capture cross-section used in the code can therefore be written in matrix form as

$$\boldsymbol{\sigma}_{\text{capt}} = \sum_{\text{MT}=102}^{107} \boldsymbol{\sigma}_{\text{MT}} + \boldsymbol{E}\boldsymbol{\sigma}_{16} = \boldsymbol{S}\boldsymbol{\sigma} \tag{23}$$

where $\boldsymbol{E} \in \mathbb{R}^{G\times G} : E_{11} = 1,\ E_{ij} = 0$ otherwise; $\boldsymbol{S} \in \mathbb{R}^{G\times 7G}$ and the vector $\boldsymbol{\sigma}$ contains the concatenated reaction-specific cross-sections. Since the relationship between $\boldsymbol{\sigma}_{\text{capt}}$ and $\boldsymbol{\sigma}$ is linear, the absolute covariance matrix corresponding to $\boldsymbol{\sigma}_{\text{capt}}$ can be accurately computed with the Sandwich rule:

$$\text{Cov}[\boldsymbol{\sigma}_{\text{capt}}] = \boldsymbol{S}\text{Cov}[\boldsymbol{\sigma}]\boldsymbol{S}^T. \tag{24}$$

Notice that this treatment does not involve any approximation in the Bayesian framework, if all the probability distributions are assumed to be Gaussian, which is a standard practice in nuclear data uncertainty analysis. The corresponding relative covariance matrix can then be easily calculated by dividing the covariance matrix elements C_{ij} by $\sigma_i\sigma_j$, i.e. by dividing the covariance matrix element-wise by the matrix $\boldsymbol{\sigma} \otimes \boldsymbol{\sigma}$. Fig. 1 shows an example of this treatment for the capture reactions of ^{16}O.

After forming the covariance matrices for the capture cross-sections, they can be used in both deterministic and statistical uncertainty analysis. In the deterministic case, the sensitivities with respect to the capture cross-sections can be computed in the usual manner according to Eq. (8). Notice that apart from the (n,2n) reaction, this approach should give results that are consistent with those obtained by computing the sensitivities with respect to the individual capture reactions.

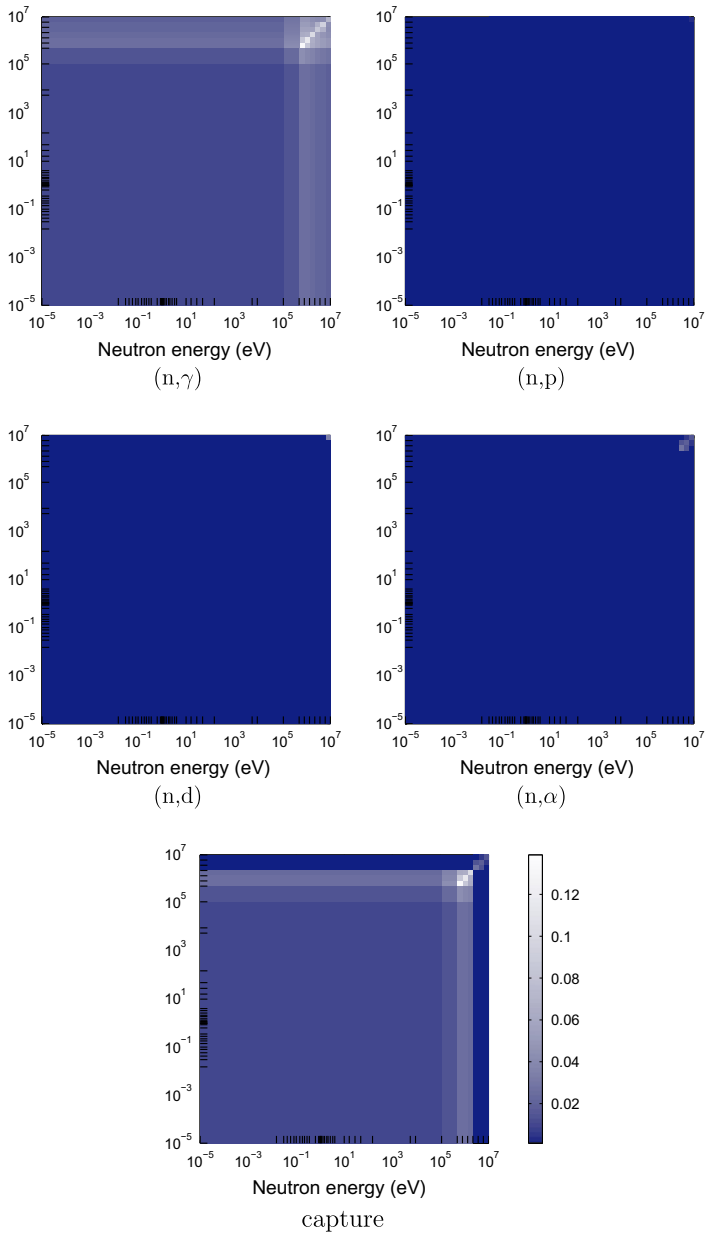

Fig. 1. Covariance matrices corresponding to the individual capture cross-sections and the total capture cross-section of ^{16}O. The covariance matrices in this example are from the SCALE 5.1 covariance library `44groupv6rec` and they have been processed to conform to the energy-group structure of CASMO-4.

3.2.3. S&U analysis of scattering cross-section

Dealing with scattering cross-sections is more complicated. In general, there are no covariance data available for transfer cross-sections $\sigma_x^{h\to g,j}$ but only for $\sigma_x^{g,j}=\sum_{h=1}^{G}\sigma_x^{g\to h,j}$, where x refers to a scattering reaction (e.g. elastic, inelastic) and j is the nuclide index. However, because of the scattering source term in Eq. (13), the derivative with respect to $\sigma_x{}^{g,j}$ is not mathematically well-defined without additional constraints. Typically it is assumed that the probabilities of transfers to various groups are fixed, i.e.

$$\sigma_x^{g\to h,j}=\sigma_x^{g,j}p_x^{g\to h,j} \tag{25}$$

where $p_x^{g\to h}$ is the proportion of neutrons scattered from energy group g to energy group h, which is assumed to remain fixed even if the scattering cross-section $\sigma_x^{g,j}$ is perturbed (Weisbin et al., 1976). Based on this assumption, the scattering source in Eq. (13) can be written

$$S^g=\frac{1}{4\pi}\sum_{h=1}^{G}\Sigma_s^{h\to g}\phi^h=\frac{1}{4\pi}\sum_x\sum_j N^j\sum_{h=1}^{G}\sigma_x^{h,j}p_x^{h\to g}\phi^h \tag{26}$$

where the summations over x include all scattering reactions. After this assumption, the derivative with respect to $\sigma_x^{g,j}$ is well-defined and can be computed as usual. It is straightforward to show that this approach corresponds to computing the sensitivity coefficients with respect to the transfer cross-sections $\sigma_x^{g\to h,j}$ and summing them over h.

Unfortunately, the sensitivity with respect to the total scattering cross-section $\sigma_s^j = \sum_x \sigma_x^j$ is not well-defined if the constraint (25) is enforced. Instead, fixed transfer rates must be assumed for the total scattering cross-section, which is clearly a stricter assumption than Eq. (25). Mathematically, this approach corresponds to computing the relative sensitivities with respect to the individual scattering reactions and adding them up. It should be emphasized that because the sensitivity coefficients corresponding to the total and individual scattering reactions are based on inconsistent assumptions, the chain rule of derivation is not applicable to these sensitivities. Therefore, it is not possible to perform S&U analysis with respect to the total scattering cross-section in a manner that would produce results consistent with the approach where the sensitivities are computed with respect to the individual scattering reactions. Nonetheless, the covariance matrices for the individual scattering reactions can be combined in a similar manner as the capture reactions. However, it should be kept in mind that both these approaches are in fact based on simplifications of the true problem and are likely to underestimate the uncertainty related to scattering cross-sections.

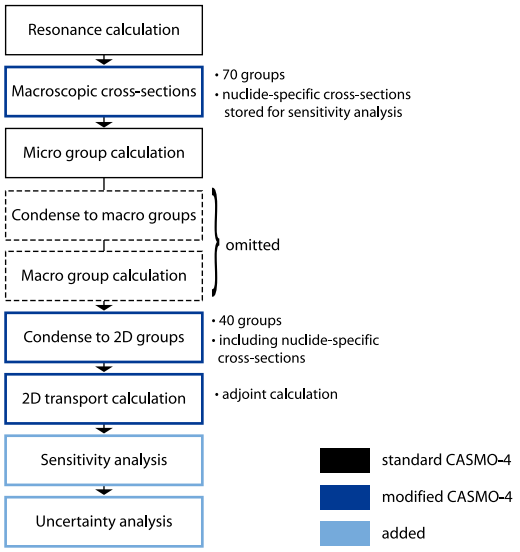

Fig. 2. Outline of the CASMO-4 calculations.

4. Results

The calculation framework was applied to two test cases from the UAM benchmark Exercise 1.1 (Ivanov et al., 2011). The first test problem represents TMI-1 under hot zero power conditions and the second one is a GEN-III MOX pin-cell test case with 9.8% of plutonium. These test problems were chosen to be presented here because they can also be modeled in one dimension and therefore the results can be compared against TSUNAMI-1D (Rearden, 2009) In addition, based on experiments with other pin-cell test cases included in the UAM benchmark specification, the chosen test cases are highly representative and characteristic in terms of comparison to TSUNAMI-1D. The developed CASMO-4 calculation system is naturally also well-suited for fuel assembly calculations, but because the S&U results for pin-cell and lattice problems are essentially very similar, only the 1D results were chosen to be presented here due to the possibility to validate them by comparison to TSUNAMI-1D.

The outline of the CASMO-4 calculations is presented in Fig. 2. The calculations were carried out using the cross-section library E60200 that contains 70 energy groups and is based on ENDF/B-VI data (Rhodes, 2005). The covariance data were taken from the SCALE 6 library ZZ-SCALE6.0/COVA-44G (NEA Data Bank, 2011), which is the most comprehensive covariance library available at the time of writing. The library is based on true evaluations from various sources (including ENDF/B-VII, ENDF/B-VI, JENDL-3.1) and approximate covariance data. The covariances in the library are given in relative terms and therefore the library is intended to be used with all cross-section libraries including the ones that are inconsistent with the evaluations. While this is not strictly correct, it is considered to be acceptable due to the scarcity of comprehensive covariance data among other reasons (Williams et al., 2009).

The list of the nuclides present in these test cases can be found in the benchmark specification (Ivanov et al., 2011). Apart from the isotopes of Cr and Fe, all available covariance data in the library was included in the uncertainty computations. The reason for excluding these isotopes is that the employed cross-section library E60200 does not contain isotope-specific cross-sections for these materials. For this same reason, the given nuclide composition could not be specified for the zircalloy-4 cladding in the MOX test case, but was instead replaced by the zircalloy-4 composition given for the PWR test case.

The covariance matrices from ZZ-SCALE6.0/COVA-44G were processed for compatibility with CASMO-4. The sensitivity profiles in CASMO-4 were computed using the 40-group structure option that was the closest match to the amount of groups in the covariance data and, as mentioned in Section 3.2, the code Angelo 2.3 (Kodeli, 2010) was used to process the covariance matrices to this energy-group structure. Next, the nuclear data processing code NJOY (MacFarlane and Muir, 1994) was used to transform the 40-group covariance files to the BOXR format. Auxiliary FORTRAN programs were written for combining the covariance matrices according to the principles described in Section 3.2.

The TSUNAMI-1D calculations were performed using the ENDF/B-VI-based cross-section library V6-238 containing 238 energy groups. The module CENTRM was used for self-shielding. Implicit sensitivity analysis (Williams et al., 2001) was omitted in the TSUNAMI calculations in order to facilitate the comparison of the results given by CASMO-4 and TSUNAMI-1D. The boundary conditions for the 1D models were assumed to be white, whereas reflective boundary conditions were used for the 2D-calculations with CASMO-4.

4.1. PWR pin-cell

A summary of the numerical results for the PWR pin-cell representing TMI-1 is presented in Table 1. The relative difference between the multiplication factors computed with CASMO-4 and TSUNAMI-1D is 0.1763% in the forward case and 0.1768% in the

Table 1
Summary of the results for the PWR pin-cell test case.

Code	Forward k	Adjoint k	Rel. uncertainty, $\frac{\Delta k}{k}$ (%)
CASMO-4	1.421684	1.421686	0.5120
TSUNAMI-1D	1.419177	1.419172	0.4888

Table 2
The ten most significant sources of uncertainty in the PWR pin-cell test case and the corresponding energy-and region-integrated relative sensitivity coefficients. The sensitivity coefficients with respect to the parameter χ have been constrained according to Eq. (22).

Nuclide	Parameter pair	Sensitivity, CASMO	Sensitivity, TSUNAMI	Contribution to $\frac{\Delta k}{k}$ (%), CASMO	Contribution to $\frac{\Delta k}{k}$ (%), TSUNAMI
^{238}U	σ_c, σ_c	-2.609×10^{-1}	-2.219×10^{-1}	3.253×10^{-1}	2.836×10^{-1}
^{235}U	$\bar{\nu}$, $\bar{\nu}$	9.379×10^{-1}	9.392×10^{-1}	2.641×10^{-1}	2.643×10^{-1}
^{235}U	σ_c, σ_c	-1.549×10^{-1}	-1.539×10^{-1}	2.225×10^{-1}	2.098×10^{-1}
^{235}U	σ_c, σ_f			1.087×10^{-1}	1.039×10^{-1}
^{235}U	χ, χ	2.166×10^{-6}	-3.581×10^{-9}	8.345×10^{-2}	8.774×10^{-2}
^{235}U	σ_f, σ_f	2.559×10^{-1}	2.538×10^{-1}	7.838×10^{-2}	7.652×10^{-2}
^{238}U	$\bar{\nu}$, $\bar{\nu}$	6.210×10^{-2}	6.076×10^{-2}	7.225×10^{-2}	7.122×10^{-2}
Zr	σ_c, σ_c	-9.403×10^{-3}	-8.315×10^{-3}	6.195×10^{-2}	5.070×10^{-2}
^{238}U	σ_s, σ_s	-5.858×10^{-3}	-6.178×10^{-3}	3.941×10^{-2}	1.058×10^{-1}
^{1}H	σ_s, σ_s	1.952×10^{-1}	1.866×10^{-1}	2.739×10^{-2}	2.581×10^{-2}

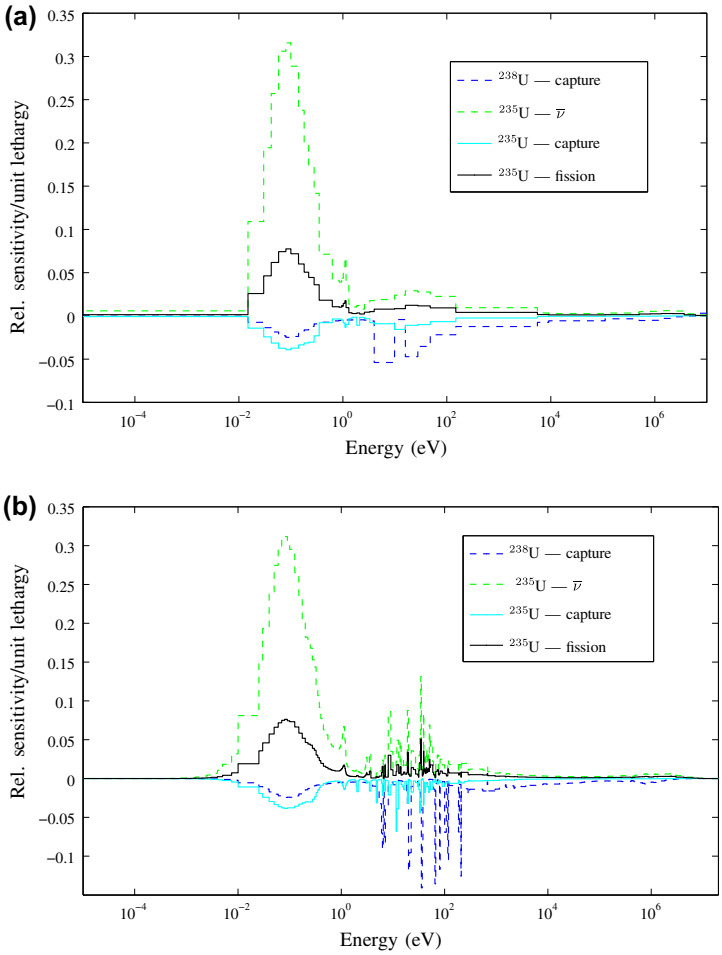

Fig. 3. Sensitivity profiles for the PWR pin-cell test case computed with (a) CASMO-4 and (b) TSUNAMI-1D.

adjoint case. For the total uncertainty, on the other hand, the value given by CASMO is 4.531% greater. Table 2 shows the ten most significant sources of uncertainty together with the corresponding energy-and region-integrated sensitivity coefficients. It can be seen from this Table that in both calculations the main contribution to the total uncertainty comes from the capture cross-section of ^{238}U, which is characteristic of LWR calculations with UOX. Also, the difference in the total uncertainties is mainly attributable to the fact that the CASMO calculation yields greater sensitivities for this cross-section. This appears to originate from the differences in the cross-section libraries. In particular, the cross-section library `E60200` used in the CASMO calculation has not been

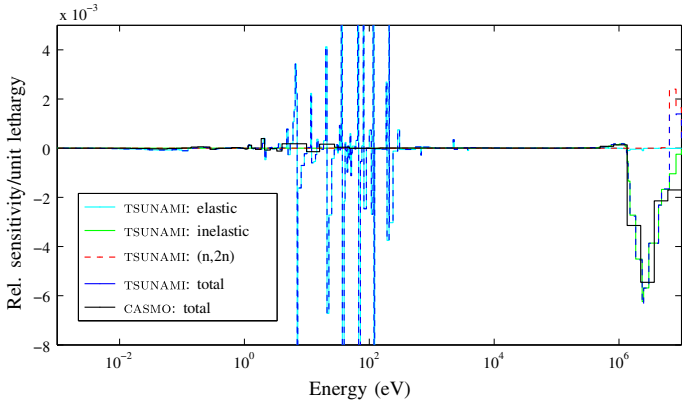

Fig. 4. Closeup of scattering sensitivity profiles of ^{238}U in the PWR pin-cell test case.

Table 3
Summary of the results for the MOX pin-cell test case.

Code	Forward k	Adjoint k	Rel. uncertainty, $\frac{\Delta k}{k}$ (%)
CASMO-4	1.09964	1.09964	0.9156
TSUNAMI-1D	1.09493	1.09495	0.9338

reduced in terms of the ^{238}U resonance integral, which is known to be overestimated in the ENDF/B-VI data (Rhodes, 2005). The ^{238}U capture sensitivity profile and some other sensitivity plots of interest are shown in Fig. 3.

From Fig. 3 and Table 2, it can be seen that, overall, the results between CASMO-4 and TSUNAMI-1D are in good accordance. It should be noticed that the ^{235}U fission spectrum sensitivities in Table 2 have been constrained according to Eq. (22). Therefore these values should theoretically vanish and the non-zero values result from round-off errors. In particular, the single-precision arithmetics used in CASMO-4 produces a greater deviation. Other than this, the only notable difference in the uncertainty results occurs for the scattering cross-section of ^{238}U, which is due to the inconsistency in defining the sensitivities, as discussed in Section 3.2. The corresponding scattering sensitivities are plotted in Fig. 4. Notice that in some energy groups the reaction-specific scattering sensitivities have opposite signs, which is in clear contradiction with the chain rule of derivation.

4.2. MOX pin-cell

The results for the MOX pin-cell test case are summarized in Table 3. In the forward case, the relative difference between the multiplication factors computed with CASMO-4 and TSUNAMI-1D is 0.4283%. In the adjoint case, the respective relative difference is 0.4265%. For this test case, TSUNAMI-1D gives a greater uncertainty with a relative difference of 1.988%. The ten covariance matrices that contributed the most to the multiplication factor uncertainty are shown in Table 4 together with the corresponding energy-and region-integrated sensitivity coefficients. In addition, the sensitivity profiles of the five most significant sources of uncertainty are plotted in Figs. 5 and 6.

It can be seen from Table 4 that the main contribution to the total uncertainty in both CASMO-4 and TSUNAMI-1D calculations comes from the parameter $\bar{\nu}$ of ^{239}Pu. The capture cross-section of ^{238}U is another significant contributor to the total uncertainty. Similarly to the PWR pin-cell calculation, CASMO-4 yields a greater sensitivity for this cross-section, causing a greater contribution to the total uncertainty. The most notable difference in the results occurs for the capture reaction of ^{242}Pu, for which CASMO-4 yields a significantly greater sensitivity, and consequently a greater uncertainty. The respective sensitivity profiles, as computed with both codes, are shown in Fig. 6. Although the integrated value of TSUNAMI-1D is about 33% smaller, it can be seen from this figure that qualitatively the sensitivity profiles are very similar. The cause of the inconsistency in the sensitivities is not evident, but it may be related to differences in both the cross-section libraries as well as the self-shielding treatment of ^{242}Pu. As an example of the latter's effect on the sensitivity, computing the same test case using SCALE 5.1 with the module NITAWL for self-shielding, resulted in a 6.493% greater sensitivity value than the one given by SCALE 6 with the module CENTRM.

Another relevant difference in the results occurs again for the scattering cross-section of ^{238}U, which is due to the discussed inconsistency in defining the sensitivities. It is noteworthy that

Table 4
The ten most significant sources of uncertainty in the MOX pin-cell test case and the corresponding energy-and region-integrated relative sensitivity coefficients. The sensitivity coefficients with respect to the parameter χ have been constrained according to Eq. (22).

Nuclide	Parameter pair	Sensitivity, CASMO	Sensitivity, TSUNAMI	Contribution to $\frac{\Delta k}{k}$ (%), CASMO	Contribution to $\frac{\Delta k}{k}$ (%), TSUNAMI
^{239}Pu	$\bar{\nu},\bar{\nu}$	7.212×10^{-1}	7.251×10^{-1}	7.273×10^{-1}	7.311×10^{-1}
^{238}U	σ_c,σ_c	-1.963×10^{-1}	-1.611×10^{-1}	2.457×10^{-1}	2.078×10^{-1}
^{242}Pu	σ_c,σ_c	-2.339×10^{-2}	-1.557×10^{-2}	2.339×10^{-1}	1.359×10^{-1}
^{239}Pu	σ_f,σ_f	3.619×10^{-1}	3.596×10^{-1}	2.236×10^{-1}	2.204×10^{-1}
^{239}Pu	σ_c,σ_c	-1.974×10^{-1}	-2.004×10^{-1}	1.960×10^{-1}	1.928×10^{-1}
^{239}Pu	χ,χ	-5.462×10^{-7}	5.672×10^{-9}	1.640×10^{-1}	1.997×10^{-1}
^{239}Pu	σ_c,σ_f			1.555×10^{-1}	1.582×10^{-1}
^{240}Pu	σ_c,σ_c	-1.104×10^{-1}	-1.052×10^{-1}	1.549×10^{-1}	1.459×10^{-1}
^{238}U	σ_s,σ_s	-1.591×10^{-2}	-1.494×10^{-2}	9.952×10^{-2}	2.721×10^{-1}
^{238}U	$\bar{\nu},\bar{\nu}$	8.333×10^{-2}	8.165×10^{-2}	9.668×10^{-2}	9.534×10^{-2}

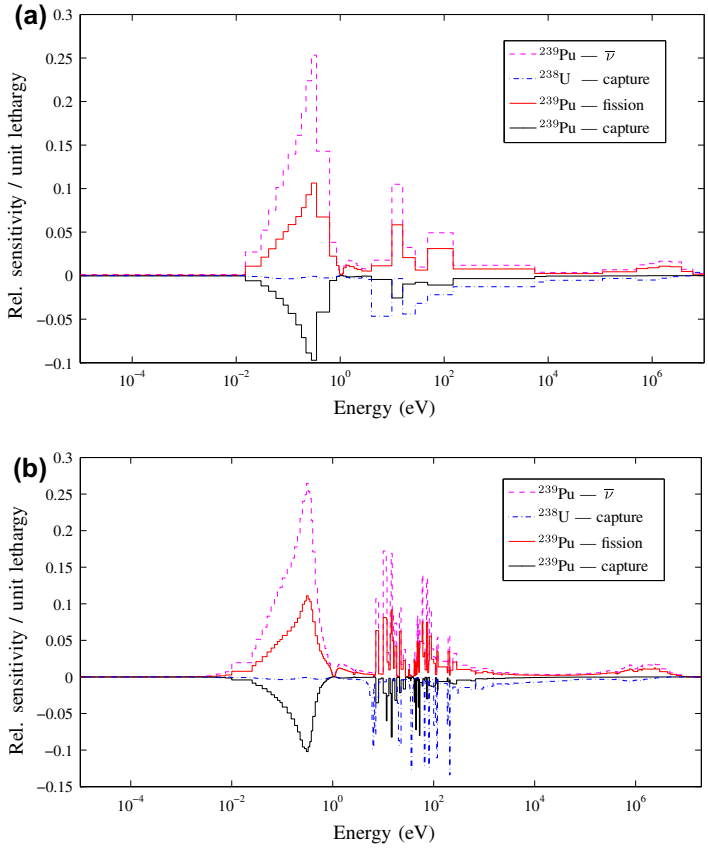

Fig. 5. Sensitivity profiles for the MOX pin-cell test case computed with (a) CASMO-4 and (b) TSUNAMI-1D.

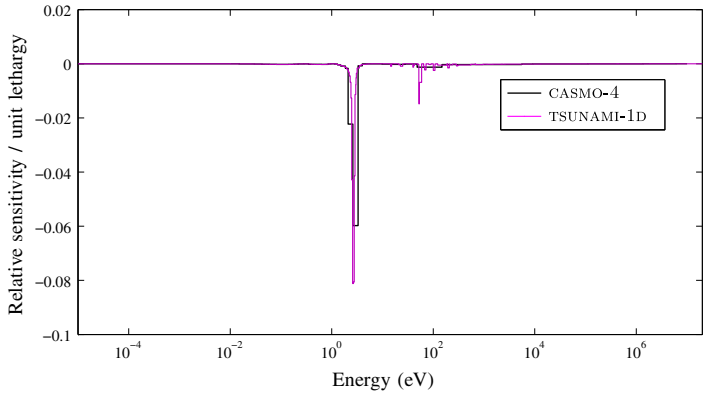

Fig. 6. Sensitivity profiles for the total capture cross-section of ^{242}Pu in the MOX pin-cell test case.

in this test case this inconsistency has a more pronounced effect on the overall results compared to the PWR test case. This is due to the harder neutron spectrum of MOX fuel, which increases the sensitivity of the multiplication factor to the inelastic scattering of ^{238}U. In the TSUNAMI-1D computation, this parameter is actually the second most significant source of uncertainty, contributing 2.703×10^{-1}% to the total uncertainty, whereas the contribution from the respective total scattering is only 9.952×10^{-2}% in the

CASMO-4 calculation. The fact that TSUNAMI-1D gives a greater total uncertainty for the multiplication factor is mainly attributable to this.

5. Summary and conclusions

The motivation of the presented work has been participating in the UAM benchmark, whose first stage aims at propagating the uncertainty related to neutron cross-sections through a reactor physics calculation. CASMO-4 was chosen as the development platform due to its role as the standard code at VTT Technical Research Centre of Finland.

As a first development, classical perturbation theory has been implemented to CASMO-4, which has enabled performing sensitivity analysis of the multiplication factor. In the process of modifying CASMO-4, a problem was faced due to the incompatibility of the cross-section models between the covariance libraries and the code itself because in CASMO-4, the individual capture and scattering cross-sections have been combined into total capture and scattering cross-sections. This issue affects all similar reactor physics codes irrespective of the method used for S&U analysis, whether deterministic or statistical. As a solution to this discrepancy, a technique for combining the covariance matrices of the individual subreactions and computing the sensitivities with respect to the combined reactions was devised and applied with success. The technique accurately combines the capture reactions in a consistent manner, but the combination of the scattering reactions resulted in some systematic differences in comparison to TSUNAMI-1D. This observation drew attention to the basic assumptions that must be made in dealing with scattering reactions. The observed differences were eventually explained by the incompatible constraints in the calculation process, which in turn caused the chain rule of derivation not being applicable.

Inspired by the experiences gained in the process, the theoretical background of S&U was reviewed and presented in detail, and practical considerations were also discussed to benefit readers interested in implementing perturbation analysis capabilities to reactor physics codes. Numerical results were presented for fuel pin-cell test problems representing a PWR and a GEN-III core with MOX fuel, and the results were compared against TSUNAMI-1D. The comparison supported the observations made on the developed methodology, i.e. the results were consistent except for scattering reactions, where systematic differences appeared in cases where multiple scattering reactions were present.

At the time of writing, the work in the benchmark has continued by implementing generalized perturbation theory to CASMO-4, which enables performing S&U analysis on other responses in addition to the multiplication factor. Future work includes the refinement and validation of the implementation. When this has been accomplished, the developed S&U calculation system enables producing uncertainty estimates for homogenized assembly data, which can in turn be propagated to coupled neutronics/thermal hydraulics calculations.

Acknowledgment

The author wishes to express her gratitude to Dr. Ivan Kodeli (Institute Jozef Stefan, Slovenia) for his invaluable help regarding the code Angelo 2.3 and the covariance libraries used in this work.

References

Bidaud, A., Marleau, G., Noblat, E., 2009. Nuclear data uncertainty analysis using the coupling of DRAGON with SUSD3D. In: International Conference on Mathematics, Computational Methods & Reactor Physics (M& C 2009).

Cacuci, D.G., 2003. Sensitivity and Uncertainty Analysis, vol. 1. Chapman & Hall/CRC.

Carlson, B.G., Lathrop, K.D., 1968. Transport theory—the method of discrete ordinates. In: Greenspan, H., Kelber, C.N., Okrent, D. (Eds.), Computing Methods in Reactor Physics. Gordon and Breach Science Publishers.

DeHart, M.D., 2009. NEWT: a new transport algorithm for two-dimensional discrete ordinates analysis in non-orthogonal geometries. In: SCALE: A Modular Code System for Performing Standardized Computer Analyses for Licencing Evaluation, Version 6. No. ORNL/TM-2005/39. Oak Ridge National Library/US Nuclear Regulatory Commission.

Greenspan, E., 1982. Sensitivity functions for uncertainty analysis. In: Lewins, J., Becker, M. (Eds.), Advances in Nuclear Science and Technology, Vol. 14. Plenum Press, New York and London.

HELIOS, 2000. Methods, Studsvik Scandpower.

Herman, M., Trkov, A. (Eds.), 2009. ENDF-6 formats manual: data formats and procedures for the evaluated nuclear data file ENDF/B-VI and ENDF/B-VII. Document ENDF-102. Report BNL-90365-2009. Brookhaven National Laboratory.

Ivanov, K., Avramova, M., Kamerow, S., Kodeli, I., Sartori, E., 2011. Benchmark for Uncertainty Analysis in Modeling (UAM) for Design, Operation, and Safety Analysis of LWRs. vol. I: Specification and Support Data for the Neutronics Cases (Phase I). Version 2.0 (NEA/NSC/DOC(2011)).

Kodeli, I., Sartori, E., 1990. Neutron cross-section covariance data in multigroup form and procedure for interpolation to users' group structures for uncertainty analysis applications. In: International Conference on the Physics of Reactors: Operation, Design and Computation (PHYSOR 1990).

Kodeli, I., Ishikawa, M., Aliberti, G., 2008. Evaluation of fission spectra uncertainty and their propagation, Appendix C In: OECD/NEA WPEC Subgroup 26 final report: Uncertainty and target accuracy assessment for innovative systems using recent covariance data evaluations. OECD.

Kodeli, I., 2010. Manual for ANGELO2 and LAMBDA Codes. NEA-1798/03 Package.

Lewis, E.E., Miller Jr., W.F., 1984. Computational Methods of Neutron Transport. John Wiley & Sons.

MacFarlane, R.E., Muir, D.W., 1994. The NJOY Nuclear Data Processing System, Version 91, Manual. Los Alamos National Laboratory (LA-12740-M).

Marleau, G., Hébert, A., Roy, R., 2009. A User Guide for DRAGON Version 4. (IGE294) <http://www.polymtl.ca/nucleaire/DRAGON/>.

NEA Data Bank, 2011. ZZ-SCALE6.0/COVA-44G, a 44-group cross section covariance matrix library retrieved from the SCALE 6.0 package. (USCD1236/03).

Rearden, B.T., 2009. TSUNAMI-1D: Control module for one-dimensional cross-section sensitivity and uncertainty analysis for criticality. In: SCALE: A Modular Code System for Performing Standardized Computer Analyses for Licencing Evaluation, Version 6. No. ORNL/TM-2005/39. Oak Ridge National Library/US Nuclear Regulatory Commission.

Rearden, B.T., 2009. TSUNAMI-3D: control module for three-dimensional cross-section sensitivity and uncertainty analysis for criticality. In: SCALE: A Modular Code System for Performing Standardized Computer Analyses for Licencing Evaluation, Version 6. No. ORNL/TM-2005/39. Oak Ridge National Library/US Nuclear Regulatory Commission.

Rhodes, J., Edenius, M., 2001. CASMO-4, a fuel assembly burnup program, users manual. Studsvik of America (SSP-01/400 Rev 4, proprietary).

Rhodes, J., 2005. JEF 2.2 and ENDF/B-VI 70 group neutron data libraries. Studsvik Scandpower (SSP-04/454 Rev 2, proprietary).

Weisbin, C.R., et al., 1976. Application of FORSS sensitivity and uncertainty methodology to fast reactor benchmark analysis. Tech. Rep. (ORNL/TM-5563).

Wieselquist, W.A., Vasiliev, A., Ferroukhi, H., 2011. Towards an uncertainty quantification methodology with casmo-5. In: The International Conference on Mathematics and Computational Methods applied to Nuclear Science and Engineering (M& C 2011).

Williams, M.L., 1986. Perturbation theory for nuclear reactor analysis. In: Ronen, Y. (Ed.), CRC Handbook of Nuclear Reactors Calculations, vol. 3. CRC Press.

Williams, M.L., Broadhead, B.L., Parks, C.V., 2001. Eigenvalue sensitivity theory for resonance-shielded cross sections. Nuclear Science and Engineering 138, 177–191.

Williams, M.L., Wiarda, D., Arbanas, G., Broadhead, B.L., 2009. Scale nuclear data covariance library. In: SCALE: A Modular Code System for Performing Standardized Computer Analyses for Licencing Evaluation, Version 6. No. ORNL/TM-2005/39. Oak Ridge National Library/U.S. Nuclear Regulatory Commission.

WIMS9A, 2005. New Features, A Guide to the New Features of WIMS Version 9A <http://www.sercoassurance.com/answers/>.